SNOWSAMPLER: AN AUTONOMOUS UNCREWED AERIAL VEHICLE FOR PENETRATION-BASED SNOW STRATIGRAPHY MEASUREMENTS ON STEEP SLOPES

Claudio Chies[1,*], Tiziano Di Pietro[2], Jaeyoung Lim[1], Florian Achermann[1], Roland Siegwart[1]

[1]*Autonomous System Lab, ETH Zürich, Switzerland*
[2]*WSL-Institut für Schnee- und Lawinenforschung SLF, Davos, Switzerland*

ABSTRACT: Snow stratigraphy measurements provide important information for determining snowpack stability. However, acquiring these measurements, especially on high-aspect slopes, remains a high-risk task due to the exposure of the operator to the intrinsic avalanche hazard. Therefore, to date, little to no snow stratigraphy measurements have ever been acquired on high-risk slopes. In this work, we propose a novel solution that combines an autonomous aerial robotic system that can deploy an SMP-like measurement device into steep slopes. We achieve this by using an adaptive landing leg that allows reliable autonomous landing and taking off from steep slopes of up to 45 degrees. The vehicle uses a digital elevation map to automatically orient the vehicle's heading and landing gear. We evaluated our system on a deployment over two snow-covered slopes located in Davos, Switzerland. We demonstrated that the vehicle can successfully take snow stratigraphy measurements by landing on arbitrary locations on the terrain up to 38 degrees.

Keywords: Snow Stratigraphy, UAS, Robotics System, Slope Landing

1. INTRODUCTION

Snow stratigraphy, representing the hardness of the internal layers of the snowpack, provides crucial information on assessing avalanche risk levels and the processes of avalanche formation (Greene et al., 2010). Measuring the spatial and temporal evolution of how the weak layers develop into an avalanche would greatly enhance the understanding of avalanche formation. To that end, snow stratigraphy measurements can be acquired by penetration-based measurement devices such as the Rammsonde and Snow Micro Pen® (SMP) (Schneebeli et al., 1999), or remote measurement devices such as ground penetrating radar (GPR) (Vergnano et al., 2022). However, measurements mainly have been relying on penetration-based devices such as the SMP due to its high accuracy profile measurements. Remote measurement approaches such as GPR result in low-depth resolution measurements potentially missing thin hard layers (McCammon and Schweizer, 2002; Frauenfelder et al., 2022) that are crucial for avalanche risk assessment.

Despite the usefulness of snow stratigraphy measurements, data on the evolution of the snow layers toward avalanche formation is still rare. This is mainly due to the time and risk required by the observer to reach the measurement location. An observer (who usually also is accompanied by at least a second person) usually does not take more than a few profiles per day. Previous studies have investigated slope scale spatial variability of snow mechanical properties (Schweizer and Bellaire, 2009; Meloche et al., 2024). However, measurement locations with high avalanche risk are avoided, to minimize the risk the operator is exposed to. However, given the variable distribution of snow height across different slopes due to different expositions to wind and sun, the chosen measurement location might not be representative for the whole slope of interest. Therefore, there is a need for a method which allows acquiring high spatial and temporal resolution snow stratigraphy measurements in potentially dangerous slopes without exposing the operator to the intrinsic risk of accessing such locations.

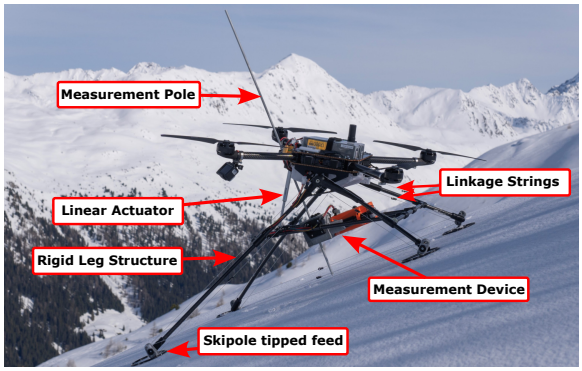

Figure 1: Overview of the SnowSampler, a unmanned aerial vehicle for penetration-based snow stratigraphy measurements.

*Corresponding author address:
Claudio Chies, Autonomous System Lab, ETH Zürich,
Leonhardstrasse 21, 8092 Zürich, Switzerland;
email: claudio@chies.com

Recently, robotic systems are increasingly being used as data-gathering tools for environment monitoring (Dunbabin and Marques, 2012). In particular, easily manageable uncrewed aerial systems (UASs) have been deployed for various applications to reach hard-to-access areas (Bircher et al., 2016; Shah et al., 2020; Lim et al., 2024). Using a UAS allows acquiring snow stratigraphy measurements remotely, enabling measurements at hard-to-access locations without exposing the observer to high avalanche risk. Additionally, as the system speeds up taking measurements, enabling dense measurements across a single slope.

In this work, we propose an autonomous uncrewed aerial systen (UAS) capable of taking off and landing on steep snow-covered terrain for snow stratigraphy measurements (Fig. 1). This is achieved by using an adaptive landing gear to safely land on steep avalanche-risk slopes. After landing, the snow stratigraphy sensor is used to penetrate the snow to gather snow stratigraphy measurements. We automate the alignment process using a digital elevation map (DEM), to ensure a safe and reliable landing as well as offloading the operator workload by only specifying the measurement position.
We demonstrate the system by deploying it on two different snow-covered slopes inside the avalanche hazard area in Davos, Switzerland. We show that the system can reliably take off and land on steep snow-covered terrain, as well as operate the measurement device to gather data.

The key contribution of this work is as follows:

- Design of a fully integrated aerial robotics system capable of landing on steep snow-covered terrain.
- Equipping the robotics system with an SMP-like measurement device to gather autonomous in-situ snow stratigraphy measurements.
- Deployment and evaluation of the system in real-world snow-covered terrain.
- Demonstration of high spatial resolution in-situ measurement of snow-covered terrain.

2. RELATED WORK

2.1 Snow Stratigraphy with UAS

Existing research on drone-based automatic snow stratigraphy measurement can be divided mainly into remote sensing methods and penetration-based methods. Remote sensing methods use GPR to measure the snow layers under the snow cover by processing the reflections from the radar without making contact with the snow. GPR have recently gained interest as it can rapidly provide dense snow depth measurements over a large area (Jenssen et al., 2019; Berg-Jensen, 2021; Vergnano et al., 2022; Teisberg et al., 2022). However, GPR measurements lack the required depth resolution, as the theoretical lower bound of the measurement resolution is larger than the necessary resolution to detect weak layers (McCammon and Schweizer, 2002; Frauenfelder et al., 2022).

Penetration-based approaches use a measurement probe which is pushed into the snowpack to measure the force required to penetrate the different layers. Penetration-based devices such as the SMP (Schneebeli et al., 1999) are capable of detecting thin snow layers, due to the highly accurate depth measurement that can be associated with the high-resolution force profile. Using penetration-based measurement devices on an aerial vehicle has been explored in (Sieber et al., 2023), which uses a load cell to measure reaction forces while the drone is airborne. However, due to the quadcopter's limited degrees of freedom, its not really feasible to discard external disturbances like wind while at the same time having its movement restricted by the locked pole orientation.
In this work, we design an aerial system that operates the penetration probe after the drone has landed. This reduces the measurement noise originating from the drone. For our system, we use the SnowSoundPen, a penetration based SMP-like measurement device developed by Tiziano Di Pietro.

2.2 Landing on steep slopes

The problem of landing a drone on a steep slope has been a recurring topic for operating aerial vehicles in mountainous environments. There have been approaches with active and passive landing legs on slopes up to 20° (Baker et al., 2013) (Stolz et al., 2018). Some research present novel ideas of using reverse thrust and friction shock absorbers, with were able to achieve a safe landing on slopes up to 60° inclination (Bass et al., 2022). For larger systems, use of asymmetric landing skids have also been studied (Kim et al., 2021) where landings of up to 40° were achieved. Whereby the problem with all existing approaches is for one, they rely on friction between the feet and the surface to keep the drone in place, and are not able to compensate horizontal forces while landed. Something which we will experience during our measurement process. In this work, we design a single degree of freedom landing gear that can adjust the angle of the landing gear to safely land on steep terrain. We analyze the static stability of the landing gear geometry to ensure that the vehicle is stable during the

penetration of the snow probe.

3. SYSTEM OVERVIEW

The system has two main requirements that need to be taken into consideration. First, the vehicle should be capable of landing on slopes steeper than 30°, as avalanches form in such slopes. In this work, we focus on landing on slopes of up to 45° as steeper slopes are less relevant for snow stratigraphy. Second, the vehicle should remain stable while the sensor penetrates the snow. We assume the snow penetration probe generates up to 30 N normal force to the surface during a measurement.

The system consists of an adaptive landing gear, drone subsystem, and avionics. The adaptive landing gear is the part that adjusts the landing legs and where the sensor is mounted. The drone subsystem is the mechanical part that is related to flying the vehicle. The avionics control and stabilize system, and handle communication with the operator. The weight of the major components are listened in Table 1, where we can see that the main contributors weights wise are the drone subsystem and the batteries with 3.08 kg and 5.02 kg respectively.

3.1 Drone Subsystem

The drone subsystem is a multirotor vehicle in a quadrotor configuration, where four motors are placed on a plane. The rotors all point n the same direction, maximizing the thrust in a single direction. This configuration minimizes the required motor thrust to take off, as it is the opposite of the direction of gravity. The mass of the drone subsystem is 8.1 kg including batteries, with a dimension of 56 cm × 56 cm × 11 cm. For the propulsion T-Motor U7-V2.0 420kv BLDC motors with T-Motor AIR 40A ESCs and 17 × 6.5 propellers are used. The vehicle uses two 23000 mAh 6S Lithium Polymer Batteries. By separating the battery into two, the required maximum current of the electrical power system is divided. Considering the hover thrust power requirement, the vehicle is capable of continuously hovering for 25 minutes with a hover thrust of 65%. Then considering the total weight, this means we have an maximum thrust of 15.6 kg.

Component		**Weight**
Adaptive Landing Gear		0.72 kg
Drone Subsystem	*Batteries*	5.02 kg
	Avionics	3.08 kg
Sensor Payload		1.34 kg
Total		10.16 kg

Table 1: System components and weights

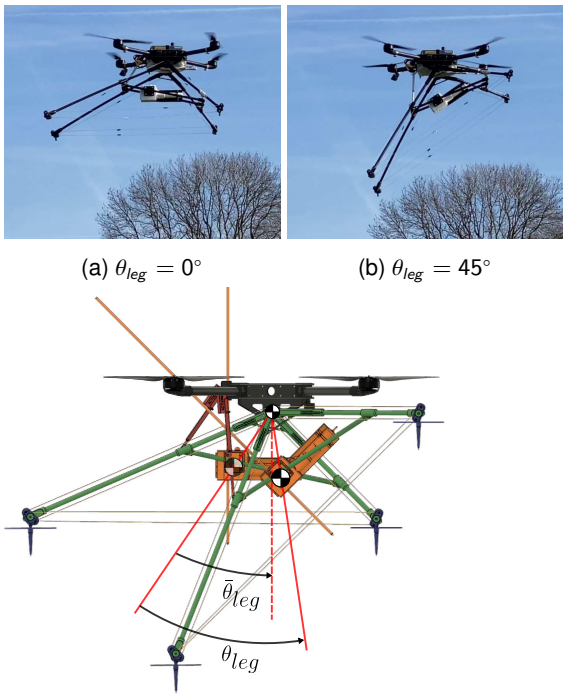

(a) $\theta_{leg} = 0°$ (b) $\theta_{leg} = 45°$

(c) Visualization of the movement at different leg angles.

Figure 2: Image of vehicle in flight with b) Level landing gear ($\theta_{leg} = 0°$) b) Full tilt ($\theta_{leg} = 45°$). c) Visualization of the movement at different leg angles. Neutral angle $\bar{\theta}_{leg}$ is defined as when the CG of the landing gear is below the CG of the drone subsystem.

3.2 Adaptive Landing Gear

The adaptive landing gear consists of a rigid frame made from carbon tubes. The measurement device is rigidly attached to the landing gear frame (Fig. 1). Four contact points are attached to the rigid frame, which form a plane. As the measurement device is rigidly mounted on the frame, this always orients the sensor normal to the surface.

The frame is then attached to the drone, through a pivot, to be able to adjust the angle of the landing gear relative to the drone subsystem. A linear actuator is used to adjust the relative angle θ_{leg}, which can be adjusted up to 45°. Fig. 2c shows the range of movement of the adaptive landing gear on the system. The advantage of adjusting the leg angles is that after landing, the motors are kept level, which reduces the required thrust to take off from the surface.

Note that as the landing gear is actuated, the center of gravity of the whole system shifts Fig. 2c. We define the neutral angle as the landing gear angle where the center of mass is centered below the geometric center of the UAV. The neutral angle for the landing leg was $\bar{\theta}_{leg} = 34.7°$, whereby the full

Figure 3: Foot design which allows taking off and landing on snow

range of motion is [0°,45°].
In order to distribute the load evenly during hover, we adjust the landing gear to a neutral position during navigation, and adjust the landing gear to the desired angle for landing.

The landing feet are custom designed and are built using ski pole tips with flexible baskets and minimize the sinking into the snow surface (Fig. 3). The flexible basket consists of a flexible ring connected with the center through strings. This allows the basket to adapt to different slope angles, while avoiding getting buried below the snow during landing. The feet are connected to the frame through a hinge, where a tensioned cord is connected to the fuselage of the drone subsystem. These cords form a linkage system, keeping the orientation of the feet fixed. This maximizes the stability of the vehicle when landing.

3.3 Avionics

The avionics system consists of an onboard computer and a flight management unit (FMU). The onboard computer is used for operating the drone subsystem, the active landing gear and the measurement device. An Intel NUC with an i7-7560U 3.5GHz processor is used as the onboard computer.
The onboard computer sends the flight commands coming from the ground station to the flight controller and also controls the linear actuator and measurement device. The communication between the groundstation and onboard computer is done via a cellular link, whereby an separate radio link can be used as an fallback. The FMU handles the low-level controls of the vehicle to stabilize the drone. In an emergency, the safety pilot will be able to control the vehicle without the onboard computer by directly controlling an RC controller.

3.4 Static Stability and Landing Gear Geometry

The geometry of the landing gear plays a big role in determining the stability of the vehicle. Therefore,

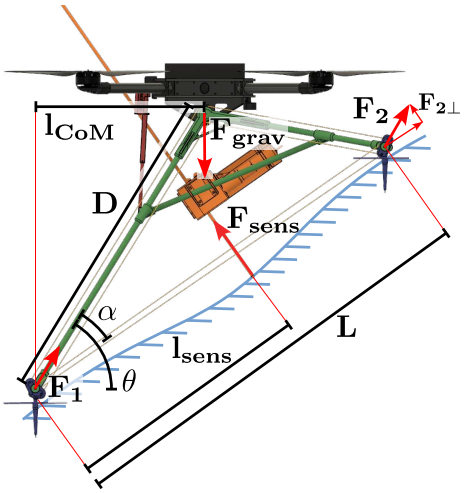

Figure 4: Force diagram and landing gear geometry for analyzing the static stability of the vehicle

we want to ensure that the vehicle can stay statically stable on the slope while operating the sensor. The key design parameters can be considered as D, L, α, which defines the geometry of the landing gear (Fig. 4). The goal is to ensure that the used geometry for the landing gear provides a static stable condition of the drone while applying the penetration force at any slope angle.

We consider the force and momentum balance at some slope inclination θ in the force diagram (Fig. 4). We denote the penetration force $\mathbf{F}_{sens}$, and the reaction forces on the feet as $\mathbf{F}_1, \mathbf{F}_2$, the gravitation force acting on the drone as $\mathbf{F}_g$. We further decompose the feet reaction forces into a normal component to the surface $\mathbf{F}_{1\perp}, \mathbf{F}_{2\perp}$ and parallel components $\mathbf{F}_{1\parallel}, \mathbf{F}_{2\parallel}$. The static stability conditions can be written as follows:

$$\vec{\mathbf{F}}_g + \vec{\mathbf{F}}_{sens} + \mathbf{F}_1 + \mathbf{F}_2 = 0 \tag{1}$$

$$\vec{\mathbf{F}}_{sens} l_{sens} + \mathbf{F}_{2\perp} L = \vec{\mathbf{F}}_g l_{CoM} \tag{2}$$

$$\vec{\mathbf{F}}_{sens} l_{sens} + \mathbf{F}_{1\perp}(L - l_{sens}) = \vec{\mathbf{F}}_g (L cos\theta - l_{CoM}) \tag{3}$$

For simplicity of notation, we denote $l_{CoM}(\theta) = Dcos(\theta + \alpha)$. As the contact force cannot hold the feet in the normal direction of the surface, the conditions in which the feet stay on the ground is when the force normal to the surface is positive.

$$\mathbf{F}_{1\perp} > 0 \quad and \quad \mathbf{F}_{2\perp} > 0 \tag{4}$$

Therefore, given the geometry of the landing gear, the static stability condition is fulfilled when Eq. (4) holds. Inferring Eq. (4) on Eq. (2) and Eq. (3) results in Eq. (5) and Eq. (6)

Parameters	Values
α	23.43°
L	102.5 cm
D	77.8 cm
l_{sens}	59.5 cm

Table 2: Landing gear geometry that satisfies the static stability condition.

$$l_{sens} < \frac{\|\mathbf{F}_g rav\| l_{CoM}(\theta)}{F_{sens}} \quad (5)$$

$$l_{sens} > L - \frac{\|\mathbf{F}_g\|(L\cos(\theta) - l_{CoM}(\theta))}{F_{sens}} \quad (6)$$

Note that as long as the above condition holds, the height of the CG does not influence the stability of the vehicle. Therefore, the height was designed to ensure that there is enough clearance (5.9 cm) between the rotors and the slope.

Since the momentum balance imposes a stricter constraint on the minimum weight, we decided to design the length of the tube connecting the lower feet to the drone body so as to achieve a balance between a larger footprint, which enhances stability when landed, and positioning it closer to the center of mass to reduce both the moment of inertia and overall weight (See section 3.2).

4. SYSTEM OPERATION

The operation of the vehicle consists of two phases. Prior to the flight, the operator uses the adaptive sampling strategy to generate a sequence of sample locations around the region of interest (ROI). The adaptive sampling approach generates sampling points that would most efficiently map the ROI with minimum uncertainty.

In the second phase, (see Fig. 5) the operator sets the location of the target sampling position from the planned sample locations. The onboard computer then utilizes the DEM to obtain the surface normal at the target location and calculates the landing leg angle and heading. When the operator commands a takeoff and Go-To, the system flies to the target location and adjust its heading to align with the terrain. Upon receiving the landing command, the system adjusts the landing legs to match the slope inclination and lands on the surface. Once landed, the operator can command a measurement, after which the entire cycle can be repeated for the next sample location. At the moment all these transitions are, for safety reasons, commanded by the operator, but they can be automated without much effort.

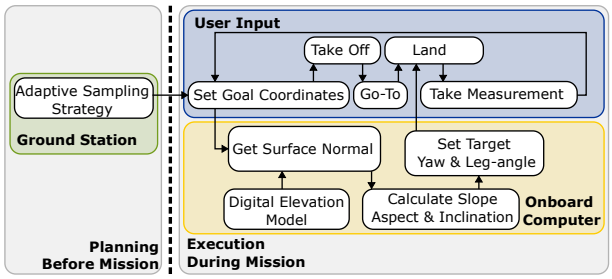

Figure 5: Flowchart showing the sampling process before and during an sampling mission.

4.1 Adaptive Sampling

Prior to the flight, we plan for which positions the measurements should be taken. As the system can navigate to arbitrary sample locations, spatially dense measurement locations can be taken along the surface. As the sampling locations are sparse, the resulting uncertainty of the slope-wise measurement will influence how the uncertainty distributes over the slope. However, determining where to sample that results in the best estimate over the whole slope can be a challenging problem. Therefore, we employ an adaptive sampling strategy, in which the sampling locations are optimized to minimize the uncertainty of the whole slope (Krause et al., 2008).

We first define a ROI, which we are interested in surveying. The ROI is defined by a polygon outline. Since the first sample is equally informative, we sample a random position inside the ROI as the first sampling location. Then we sequentially find the next-best-sample position, which maximizes the mutual information of the region inside the ROI. The next-best-sample is found by randomly sampling locations on the terrain and picking the sample location that maximizes the mutual information. The sequence is repeated until the target sample locations have been reached. Once all sampling locations are determined, the sequence of sampling locations is optimized by solving a traveling salesman problem.

Note that the mutual information-based adaptive sampling scheme does not depend on the measurement. Therefore, the sample locations can be preplanned before the flight test.

4.2 Landing on Steep Slopes

To land the vehicle in sloped terrain, the surface normal $\mathbf{n} \in \mathbb{R}^3$ and sampling position $\mathbf{p}_s \in \mathbb{R}^3$ is translated to the landing leg angle θ_{leg} and heading ψ. The calculation can be done as Eq. (7), where the subscripts represent the x, y, z components of the normal vector $\mathbf{n}$.

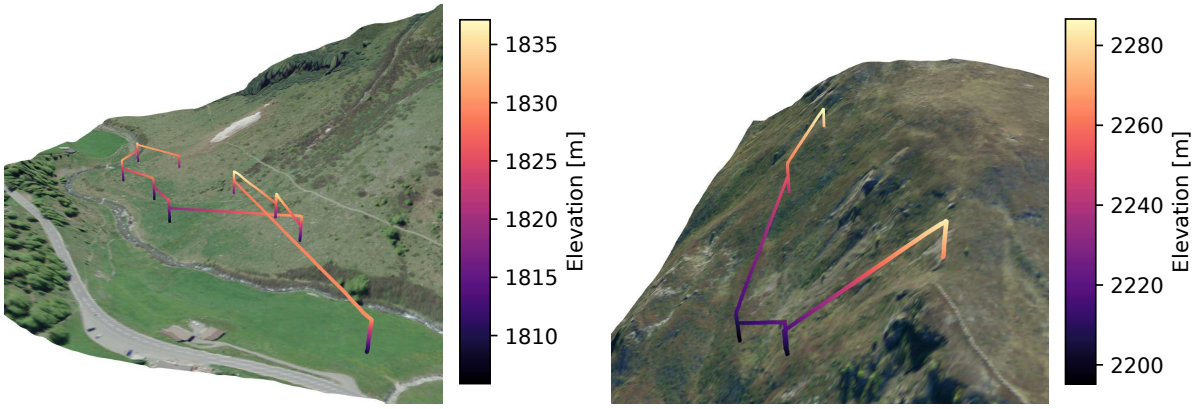

(a) 3D Flight path in *Flüelatal*

(b) 3D Flight path in *Brämabüel*

Figure 6: Flight path executed during flight tests in two different field tests (a) *Fluelatal* (b) *Brämabüel*. The altitude is colored with altitude. (swisstopo, 2024)

$$\theta_{leg} = \arctan\left(\frac{\mathbf{n}_z}{\sqrt{\mathbf{n}_x^2 + \mathbf{n}_x^2}}\right) \tag{7}$$
$$\psi = \arctan 2(\mathbf{n}_y, \mathbf{n}_x)$$

Additionally, during navigation, the vehicle keeps the landing leg at a neutral angle $\bar{\theta}_{leg}$, which places the center of gravity directly below the drone subsystem's center. This minimizes the unbalance introduced by the torque from an offset CoM, which can result in a load of motors not being evenly distributed. This can be important for long-duration flights where motor failures can occur due to thermal stress if there is an imbalanced actuation of the motors.

4.3 Navigating in Steep Alpine Terrain

The vehicle needs to be able to fly to the sample location without colliding with the terrain. To this end, the vehicle flies in a straight line between the sample locations with additional clearance altitude of 30 m.

This approach has shown to be sufficient for navigating through a slope. However, this may be insufficient in case the vehicle is operating over rugged terrain or ridges. We leave this for future work, as planning in cluttered environments is a well-established problem (Lim et al., 2024).

5. FIELD TEST RESULTS

5.1 Setup

We test our system in realistic steep alpine terrain, in two locations in Davos, Switzerland where we denote *Fluelatal* and *Brämabüel*. For both environments, we define a region of interest and the measurement points are planned through the adaptive

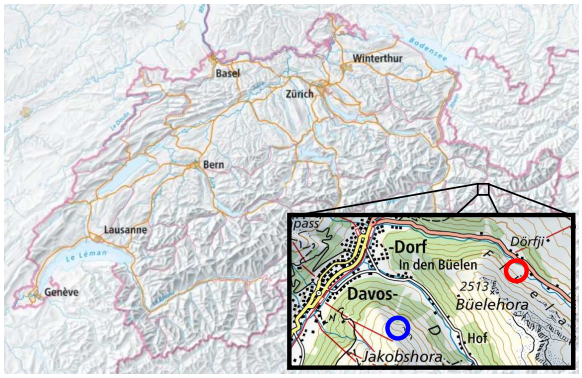

Figure 7: Test locations, whereby blue is Brämabüehl, and red is Flüelatal (swisstopo, 2024)

sampling method, as explained in section 4.1. During the experiments, the operator commands high-level commands such as take-off, initiation of go to and landing, as well as the sensor measurements. Whereby the rest is handled by the avionics stack. The aim of these experiments was to validate the performance of the System in the field, verify slope orientations and validate the hardware design.

5.2 Results

Fig. 6 shows the flight path of the vehicle during the field experiments. It can be seen that the vehicle can successfully reach various points on the snow-covered terrain. whereby, we landed autonomously on slopes up to 38° and tested the measurement device on slopes up to 45° during which the vehicle remained stable during the whole sampling process.

In Fig. 9, we see the relationship between angular error and surface inclination during the system's autonomous landings on snow. The plot shows that angular error increases with steeper inclinations, highlighting a limitation in the system's reliance on Digital Elevation Models (DEMs) for estimating

Figure 8: Onboard camera view after a successful landing in *Brämabüel*, Switzerland

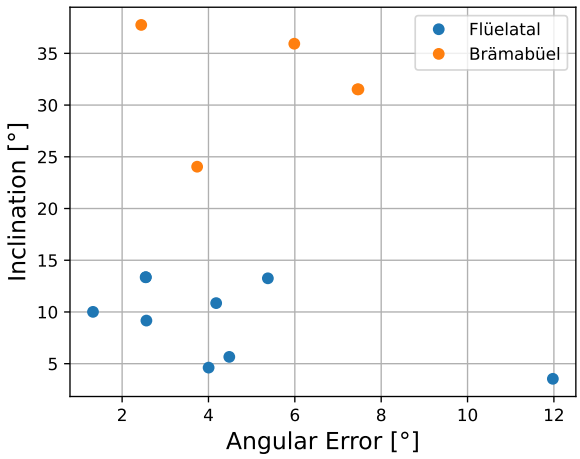

Figure 9: Angular error of the system after landing using a DEM surface orientation estimation

surface normals. Outliers at lower inclinations may also occur where snow drift fills in areas of high curvature. To improve the reliability of the system it might be beneficial to integrate depth cameras or multi-pixel LiDARs, as they can provide more accurate surface orientation data than DEMs alone.

6. DISCUSSION

In this work, we were able to show that the system can reliably take off and land on steep snow-covered slopes. The System performed well during all the tests conducted, whereby there is room for improvement regarding the size and weight of the system, as well as its software architecture. Currently, The vehicle automatically adjusts the adaptive landing gear by estimating the slope through the DEM. However, due to snow accumulation, the slope inclination might not be identical to the inclination of the DEM. While it has been shown that it is accurate enough for safe landings (Fig. 9), inaccurate estimation of the slope inclination may result in a failure to land safely. More importantly, DEMs does not include trees or obstacles, which can potentially result in the vehicle landing in unsafe locations. With the current system, the operator is responsible for making sure that the landing location is safe.

The current adaptive sampling approach plans the sampling locations prior to the flight. This is due to the fact that the uncertainty formulation used in this paper does not depend on the measurement. However, if the vehicle can access the snow stratigraphy measurement data during the mission, it could be used to incrementally plan the next sampling locations. For example, if we are trying to estimate the shape of a weak layer, we can formulate the problem as a segmentation problem using Gaussian process regression to incrementally plan the next sampling point. This would have a bigger impact on the information-gathering process, as the vehicle would be able to make a more informed-decision on where the information rich regions are for measurements.

This system has the potential to greatly reduce the associated cost and risk of taking snow stratigraphy measurements while increasing the spatial resolution of the measurements across the slope.

7. CONCLUSION

In this work, we proposed a novel mobile aerial sensor system that can safely land on steep mountainous slopes for deploying penetration-based snow stratigraphy measurement sensors. We achieve this by designing an adaptive landing gear, which can be actuated to match the inclination of the slope. We have analyzed the stability conditions the vehicle should satisfy for stable deployment. The system was demonstrated in avalanche risk slopes in Davos, Switzerland.

We expect this work to have a great impact on acquiring high-quality snow stratigraphy data, with high spatial resolution (multiple points on the slope) and high temporal resolution (multiple measurements within a day) to understand avalanche formation. The system will undergo further development to make the system more reliable and increase its autonomy.

ACKNOWLEDGEMENT

This work was supported by ETH Research Grant AvalMapper ETH-10 20-1.

References

Baker, S., Soccol, D., Postula, A., and Srinivasan, M. V.: Passive Landing Gear using Coupled Mechanical Design, 2013.

Bass, J., Tunney, I., and Desbiens, A. L.: Adaptative Friction Shock Absorbers and Reverse Thrust for Fast Multirotor Landing on Inclined Surfaces, IEEE Robotics and Automation Letters, 7, 6701–6708, doi:10.1109/LRA.2022.3176102, 2022.

Berg-Jensen, J. G.: Adaptive Monitoring of Snowpack Development using a Dynamic Linear Model., Master's thesis, NTNU, 2021.

Bircher, A., Kamel, M. S., Alexis, K., Burri, M., Oettershagen, P., Omari, S., Mantel, T., and Siegwart, R.: Three-dimensional coverage path planning via viewpoint resampling and tour optimization for aerial robots, Autonomous Robots, 40, doi:10.1007/s10514-015-9517-1, 2016.

Dunbabin, M. and Marques, L.: Robots for Environmental Monitoring: Significant Advancements and Applications, IEEE Robotics & Automation Magazine, 19, 24–39, doi:10.1109/MRA.2011.2181683, 2012.

Frauenfelder, R., Salazar, S., Dahle, H., Humstad, T., Solbakken, E., McCormack, E., Kirkhus, T., Moore, R., Dupuy, B., and Lorand, P.: Field test of UAS to support avalanche monitoring, 2022.

Greene, E., Atkins, D., Birkeland, K., Elder, K., Landry, C., Lazar, B., Mccammon, I., Moore, M., Sharaf, D., Sterbenz, C., Tremper, B., and Williams, K.: Snow, Weather, and Avalanches: Observational Guidelines for Avalanche Programs in the United States, 2010.

Jenssen, R. O. R., Eckerstorfer, M., and Jacobsen, S.: Drone-mounted ultrawideband radar for retrieval of snowpack properties, IEEE Transactions on Instrumentation and Measurement, 69, 221–230, 2019.

Kim, J., Lesak, M. C., Taylor, D., Gonzalez, D. J., and Korpela, C. M.: Autonomous Quadrotor Landing on Inclined Surfaces Using Perception-Guided Active Asymmetric Skids, IEEE Robotics and Automation Letters, 6, 7877–7885, doi:10.1109/LRA.2021.3101869, 2021.

Krause, A., Ajit, S., and Carlos, G.: Near-Optimal Sensor Placements in Gaussian Processes: Theory, Efficient Algorithms and Empirical Studies, The Journal of Machine Learning Research, 9, 235–284, doi:10.5555/1390681.1390689, URL https://dl.acm.org/doi/10.5555/1390681.1390689, 2008.

Lim, J., Achermann, F., Girod, R., Lawrance, N., and Siegwart, R.: Safe Low-Altitude Navigation in Steep Terrain With Fixed-Wing Aerial Vehicles, IEEE Robotics and Automation Letters, 9, 4599–4606, doi:10.1109/LRA.2024.3368800, 2024.

McCammon, I. and Schweizer, J.: A field method for identifying structural weaknesses in the snowpack, in: Proceedings ISSW, pp. 477–481, 2002.

Meloche, F., Gauthier, F., and Langlois, A.: Snow mechanical property variability at the slope scale – implication for snow mechanical modelling, The Cryosphere, 18, 1359–1380, doi:10.5194/tc-18-1359-2024, 2024.

Schneebeli, M., Pielmeier, C., and Johnson, J. B.: Measuring snow microstructure and hardness using a high resolution penetrometer, Cold Regions Science and Technology, 30, 101–114, doi:https://doi.org/10.1016/S0165-232X(99)00030-0, 1999.

Schweizer, J. and Bellaire, S.: Where to dig?–On optimizing sampling strategy, in: Proceedings of the International Snow Science Workshop, vol. 27, pp. 298–300, 2009.

Shah, K., Ballard, G., Schmidt, A., and Schwager, M.: Multidrone aerial surveys of penguin colonies in Antarctica, Science Robotics, 5, eabc3000, doi:10.1126/scirobotics.abc3000, URL https://www.science.org/doi/abs/10.1126/scirobotics.abc3000, 2020.

Sieber, R., Loschnigg, B., and Le Rousseau, B.: UAV-based snow stratigraphy analysis, Semester project report, URL https://www.researchgate.net/publication/371139726_UAV-based_snow_stratigraphy_analysis, 2023.

Stolz, B., Brodermann, T., Castiello, E., Englberger, G., Erne, D., Gasser, J., Hayoz, E., Muller, S., Muhlebach, L., Low, T., Scheuer, D., Vandeventer, L., Bjelonic, M., Gunther, F., Kolvenbach, H., Hopflinger, M., and Hutter, M.: An Adaptive Landing Gear for Extending the Operational Range of Helicopters, IEEE International Conference on Intelligent Robots and Systems, pp. 1757–1763, doi:10.1109/IROS.2018.8594062, 2018.

swisstopo: Map data obtained from swisstopo, Swiss Federal Office of Topography, available at https://www.swisstopo.admin.ch/en/home.html, 2024.

Teisberg, T. O., Schroeder, D. M., Broome, A. L., Lurie, F., and Woo, D.: Development of a UAV-borne pulsed ice-penetrating radar system, in: IGARSS 2022-2022 IEEE International Geoscience and Remote Sensing Symposium, pp. 7405–7408, IEEE, 2022.

Vergnano, A., Franco, D., and Godio, A.: Drone-borne ground-penetrating radar for snow cover mapping, Remote Sensing, 14, 1763, 2022.